Global and Planetary Change 229 (2023) 104238

Contents lists available at ScienceDirect

Global and Planetary Change

journal homepage: www.elsevier.com/locate/gloplacha

Temperature changes during the last deglaciation and early Holocene in southwest China

Weiwei Sun [a], Enlou Zhang [a,*], Qingfeng Jiang [b], Dongliang Ning [b], Wenlei Luo [a]

[a] State Key Laboratory of Lake Science and Environment, Nanjing Institute of Geography and Limnology, Chinese Academy of Sciences, Nanjing 210008, China
[b] School of Geography Sciences, Nantong University, Nantong 226007, China

ARTICLE INFO

Editor Name: Dr. Alan Haywood

Keywords:
Quantitative temperature reconstruction
Holocene temperature conundrum
Asian monsoon
Lacustrine sediment
Branched GDGTs

ABSTRACT

Quantitative temperature reconstructions from the Asian monsoon region may provide insight into climate forcing and help develop climate models with better prognostic potential. However, highly resolved quantitative terrestrial temperature reconstructions of the Asian monsoon domain are scarce. Here we present the results of analyses of 5-methyl and 6-methyl branched glycerol dialkyl glycerol tetraethers (brGDGTs) in lacustrine sediments from Lake Chenghai in southwest China, spanning the period 15.6–7.0 cal ka BP, to test the potential of this microbial paleothermometer. The distribution of brGDGTs changed abruptly at the end of the Heinrich 1 drought event, indicating that change in water level could overprint the temperature signal. Our reconstructed mean annual atmospheric temperature was 1–4 °C cooler than present and displayed a long-term warming trend from 14.4 to 7.0 cal ka BP. Superimposed on this overall trend, cooling events corresponding to the Older Dryas and Younger Dryas in the North Atlantic were recorded. The temperature reconstruction was in good agreement with previous brGDGT-based reconstructions and climate simulations, revealing a winter-biased and elevation-dependent mean annual atmospheric temperature change in southwest China. We suggest that the winter and summer monsoons could have played an important role in the amplification of temperature changes in high-altitude mountains and that there is a need for additional quantitative temperature records from low latitudes to help reconcile the diverging Holocene temperature trends between the different reconstructions and model data in the Asian monsoon region.

1. Introduction

The transition from a cold glaciated state to a warm interglacial period since the last glacial maximum (LGM, 26.5–19 cal ka BP) represents the most recent large-scale reorganization of the Earth's climate system (Clark et al., 2009). The examination of natural changes in climate systems can improve our understanding of climate change mechanisms and their responses to various forces. Although great efforts have been made to characterize the evolution of global temperatures from the LGM to the present, the underlying dynamics of millennial abrupt climate change during deglaciation and Holocene temperature evolution remain unclear (Liu et al., 2014; Marcott et al., 2013; Marsicek et al., 2018; Osman et al., 2021; Shakun et al., 2012). For example, using 73 marine and terrestrial records, Marcott et al. (2013) estimated global Holocene temperatures, showing a long-term cooling trend through the middle and late Holocene after the early Holocene thermal maximum. In contrast, model simulations suggest that the Holocene climate is warming because of increasing atmospheric greenhouse gas concentrations and retreating continental ice sheets, termed the Holocene temperature conundrum (Liu et al., 2014). In addition, the reconstructed Holocene temperature has a strong regional expression, with significant cooling limited to high latitudes and slight warming to low latitudes (Marcott et al., 2013). The probable causes of this spatiotemporal temperature heterogeneity include seasonal biases in proxies, the underrepresentation of terrestrial records in global temperature reconstructions, and incomplete forcing or insufficiently sensitive feedback of climate model simulations (Bader et al., 2020; Liu et al., 2014; Marsicek et al., 2018). Therefore, robust knowledge of past temperature evolution requires a better understanding of the discrepancies between individual proxy records and model data.

Pollen, chironomids, alkenones and branched glycerol dialkyl glycerol tetraethers (brGDGTs) have been widely used to reconstruct the terrestrial palaeotemperature since the LGM (Chen et al., 2020; Chu et al., 2017; Marsicek et al., 2018; Sinninghe Damsté et al., 2011;

* Corresponding author.
E-mail address: elzhang@niglas.ac.cn (E. Zhang).

https://doi.org/10.1016/j.gloplacha.2023.104238
Received 14 December 2022; Received in revised form 16 July 2023; Accepted 4 September 2023
Available online 6 September 2023

Weijers et al., 2007; Zhang et al., 2017a; Zhang et al., 2019; Zhao et al., 2021). BrGDGTs are membrane lipids produced by some bacterial species that contain straight alkyl core chains with four or six methyl groups, and one or two cyclopentyl moieties formed by internal cyclization involving a methyl group (Schouten et al., 2013; Sinninghe Damsté et al., 2011). BrGDGTs are ubiquitous in soils, peats, lacustrine sediments and marine sediments, and have great potential for use as universal paleotemperature proxies (Schouten et al., 2013; Weijers et al., 2007). With the development of chromatographic analysis, two structure isomers of the pentamethylated and hexamethylated brGDGTs have been identified, including one compound with a methyl group at position 5 and another with a methyl group at position 6 (De Jonge et al., 2014; Russell et al., 2018). Newly developed regional and global temperature calibrations based on the distributions of 5-methyl and 6-methyl brGDGTs may significantly improve the accuracy of past temperature reconstructions (De Jonge et al., 2014; Martínez-Sosa et al., 2021; Naafs et al., 2017; Russell et al., 2018; Zhao et al., 2021).

Lacustrine sediments are considered as ideal paleoclimatic archives for preserving high-resolution and continuous sedimentary sequences. Several studies on quantitative temperature records extending to the LGM have been undertaken in southwest China, where ecosystem functions and biodiversity are sensitive to global climate change (Opitz et al., 2015; Tian et al., 2019; Zhang et al., 2022; Zhang et al., 2017a; Zhang et al., 2019; Zhao et al., 2021). However, the temperature responses to millennial-scale meltwater discharge and increase in atmospheric CO_2 have been muted. For example, chironomid-based summer temperatures from Lake Tiancai display a significant cooling trend during the Holocene, whereas brGDGT-based temperatures from different altitudes show a gradual warming trend (Zhang et al., 2022; Zhang et al., 2017a; Zhang et al., 2019; Zhao et al., 2021). In addition, the most recent millennial abrupt cold event, the Younger Dryas (YD), is not identified in all of these temperature records. Therefore, it is necessary to conduct new quantitative temperature records in southwest China to improve our understanding of temperature differences and potential mechanisms since the LGM.

In this study, we present a brGDGT-based temperature record from Lake Chenghai in southwest China during the last deglaciation-Holocene transition. We focused on temperature variations when the potential

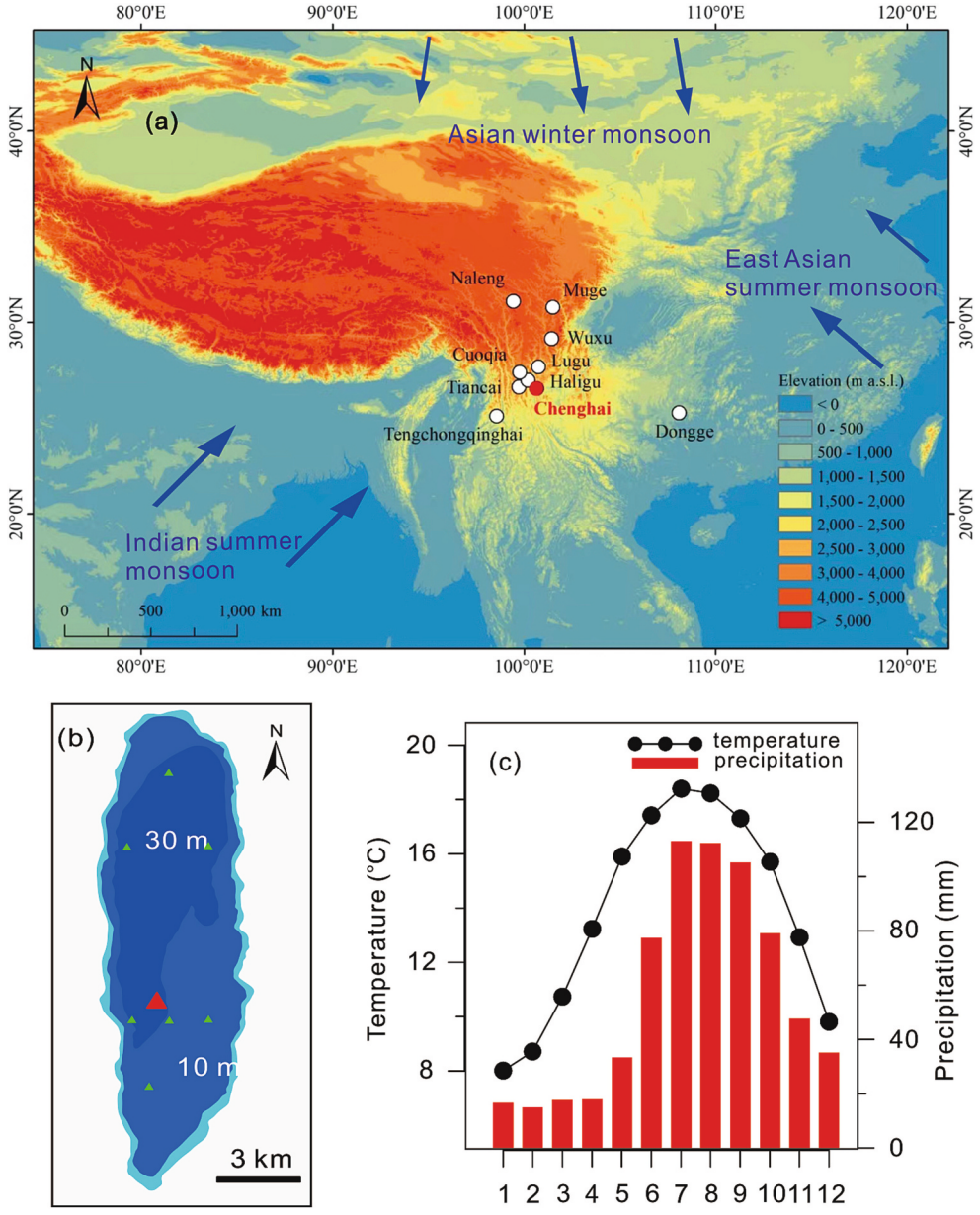

Fig. 1. (a) Map showing the location of Lake Chenghai in southwest China (triangle) and other main sites (circles): Lake Tengchongqinghai (Zhao et al., 2021); Lake Tiancai (Feng et al., 2022; Zhang et al., 2017a, 2019); Lake Haligu (Yao et al., 2020); Lake Cuoqia (Zhang et al., 2022); Lake Lugu (Zhao et al., 2021); Lake Naneng (Opitz et al., 2015); Lake Wuxu (Zhang et al., 2016); Lake Muge (Ni et al., 2019); Dongge Cave (Dykoski et al., 2005). Arrows indicate the summer and winter monsoons in the region. (b) Location of the sampling sites. (c) Mean monthly precipitation and temperature from the Yongsheng meteorological station (Xiao et al., 2018).

climate forcing rapidly changed and compared our records with the surrounding temperature records to investigate the effects of altitude and seasonality on temperature changes. We further determined the potential factors influencing temperature changes by linking high- and low-latitude processes through the Asian monsoon system.

2. Materials and methods

2.1. Site description

Lake Chenghai (26°27′–26°38′N, 100°38′–100°41′E) is a tectonic lake located in the northwest of Yunnan Province, southwest China (Fig. 1a). It is believed that Lake Chenghai was linked to the Jinsha River before the 1690s CE, and then became completely closed. The bowl-shaped terrain of the lake basin involves an altitudinal gradient from mountainous peaks with a maximum height of 3275 m above sea level (a.s.l.) to an average lake level of 1496 m a.s.l.. The lake has an area of approximately 77 km^2 and watershed area is 318 km^2 (Wu et al., 2004). The total stream channel length is very short, and most are intermittent; as a result, Lake Chenghai is naturally fed by precipitation.

This region has a subtropical climate and is influenced by the Asian summer and winter monsoons. Hydroclimatic monitoring data in the Lake Chenghai watershed show that the recent annual mean annual atmospheric temperature (MAAT) is 17.6 °C (Chen et al., 2019). The average annual precipitation is approximately 700 mm, of which approximately 80% occurs in summer and early autumn. The vegetation in the catchment is classified as Yunnan Plateau evergreen broad-leaved and pine forest. However, the present vegetation is dominated by sparse woodlands, montane shrubs, and meadows owing to human activities (Xiao et al., 2018).

2.2. Sampling and dating

In the summer of 2016, an 874-cm long composite sediment core was retrieved using a UWITEC coring platform system with a percussion corer (26°33′29.4″N, 100°39′6.7″E). The water depth was approximately 30.0 m. Each section of the core was split, photographed, and sectioned at 1-cm intervals in the laboratory. Additionally, seven surface (top 2 cm) lacustrine sediments covering the entire lake were sampled in 2014. All samples were freeze-dried prior to the analysis.

The core chronology was established using ^{14}C dating *via* accelerator mass spectrometry (AMS) (Sun et al., 2019). Seven terrestrial plant macrofossil samples were dated at the Beta Analytic Radiocarbon Dating Laboratory in Miami, USA. All AMS ^{14}C dates were calibrated to calendar years before the present (0 BP: 1950 CE) using the IntCal13 calibration data set (Reimer et al., 2013). Using the AMS ^{14}C method to date sediments from the last deglaciation is potentially problematic because terrestrial plant residues are often poorly preserved in unstable sedimentary environments (Sun et al., 2019). Because the variations in the authigenic carbonate stable oxygen isotope ($\delta^{18}O$) of the lakes were dominated by variations in the isotopic composition of lake water and monsoon precipitation in southwest China, we further correlated the authigenic carbonate $\delta^{18}O$ record of Lake Chenghai and the speleothem $\delta^{18}O$ record from Dongge Cave in southwest China (Fig. S1a, Dykoski et al., 2005; Sun et al., 2019). Although the ages in the stalagmite $\delta^{18}O$ record were within the 95% confidence interval of the original ^{14}C age-depth model, the offset between the U—Th age and the original ^{14}C age reached 400 years at the initiation of the YD event in the Indian summer monsoon region. Because the timing of the millennial-scale events was clearly comparable, we performed a visual correlation between the authigenic carbonate $\delta^{18}O$ record of Lake Chenghai and the speleothem $\delta^{18}O$ record from Dongge Cave. The uncertainties of each anchor point were evaluated by considering the resolution of $\delta^{18}O$ analysis. We obtained three $\delta^{18}O$ ages to refine the AMS ^{14}C model and study millennial climate change during the last deglaciation (Fig. S1b).

2.3. Lipid extraction and analysis

Samples for brGDGT analysis were extracted ultrasonically using a mixture of dichloromethane and methanol (9:1, *v/v*). The supernatants were condensed and hydrolyzed in 1 M KOH/methanol solution. The neutral fractions were separated into non-polar and polar fractions on a silica gel column using *n*-hexane and methanol, respectively. The polar fraction containing brGDGTs was concentrated and filtered through 0.45 μm polytetrafluoroethylene syringe filters using *n*-hexane/ isopropanol (99:1 *v/v*). These fractions were then dried in N_2 and stored at −20 °C until further analysis.

BrGDGTs were analyzed using an Agilent 1260 series high-performance liquid chromatography-atmospheric pressure chemical ionization-mass spectrometer (HPLC- APCI- MS) following the procedure described by Yang et al. (2015) at the Institute of Tibetan Plateau Research, Chinese Academy of Sciences. This method allowed the separation of 5- and 6-methyl brGDGTs. The analysis was performed in single ion monitoring (SIM) mode *via* the $[M + H]^+$ of brGDGTs (1050, 1048, 1046, 1036, 1034, 1032, 1022, 1020, and 1018) and peak areas were manually integrated. Labeling of brGDGTs followed established protocols, with Roman numbers indicating no (I), one (II), or two (III) additional methyl groups at the C5 or C6 (′) position and letters indicating none (a), one (b), or two (c) cyclopentane rings (Fig. S2; De Jonge et al., 2014). Relative abundance was calculated as the proportion of each brGDGT to the sum of all common 15 brGDGTs.

2.4. Calculation of brGDGTs-based indices

Several brGDGTs-based ratios were calculated to evaluate the applicability of brGDGTs for paleoenvironmental and paleoclimatic reconstructions of Lake Chenghai. MBT index was introduced to quantify the fractional abundances of tetramethylated brGDGTs (Ia–Ic) relative to tetramethylated, pentamethylated (IIa–IIc), and hexamethylated (IIIa–IIIc) compounds. This was calculated according to Weijers et al. (2007), as follows:

$$\mathrm{MBT} = \frac{Ia + Ib + Ic}{Ia + Ib + Ic + IIa' + IIb' + IIc' + IIIa' + IIIb' + IIIc' + IIa + IIb + IIc + IIIa + IIIb + IIIc}$$

The MBT'_{5Me} and *Index1* were calculated according to De Jone et al. (2014):

$$MBT'_{5Me} = \frac{Ia + Ib + Ic}{Ia + Ib + Ic + IIa + IIb + IIc + IIIa}$$

$$\mathrm{Index1} = log\ \frac{Ia + Ib + Ic + IIa' + IIIa'}{Ic + IIa + IIc + IIIa + IIIa'}$$

The isomerization ratio IR_{6Me} proposed by Dang et al. (2016) was used to represent the relative abundances of the 6-methyl and 5-methyl isomers:

$$IR_{6Me} = \frac{IIa' + IIb' + IIc' + IIIa' + IIIb' + IIIc'}{IIa' + IIb' + IIc' + IIIa' + IIIb' + IIIc' + IIa + IIb + IIc + IIIa + IIIb + IIIc}$$

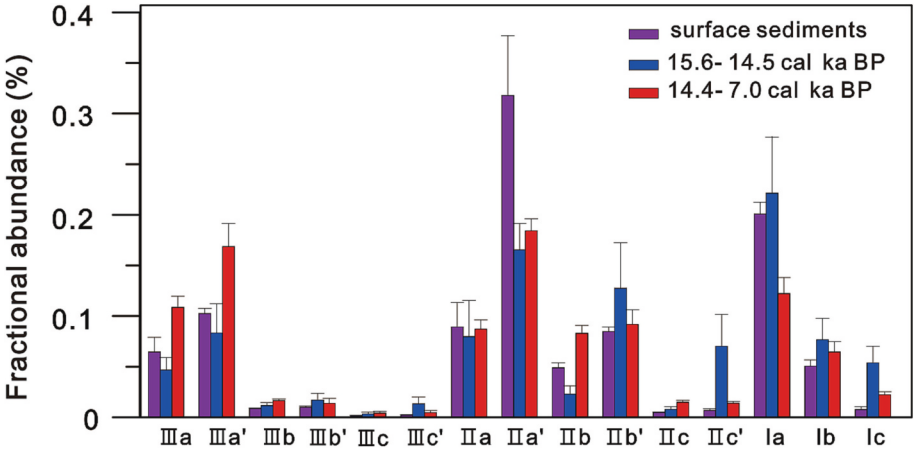

Fig. 2. Histogram showing the fractional abundance of each brGDGT in the sediments of Lake Chenghai.

We also computed the ∑IIIa/∑IIa ratio following Xiao et al. (2016):

$$\frac{\sum \mathrm{IIIa}}{\sum \mathrm{IIa}} = \frac{\mathrm{IIIa} + \mathrm{IIIa}'}{\mathrm{IIa} + \mathrm{IIa}'}$$

3. Results

BrGDGTs containing one or two cyclopentyl moieties were less abundant than those without cyclopentyl moieties, and brGDGTs were dominated by the pentamethylated series (55.2%), followed by the tetramethylated (25.9%) and hexamethylated (18.9%) brGDGT series in Lake Chenghai surface lacustrine sediments (Fig. 2). 6-Methyl brGDGTs were abundant, ranging from 39.4% to 59.0% with a mean of 52.4%. Although there was no large difference in the distribution of brGDGTs between the surface lacustrine sediments and down-core samples, the

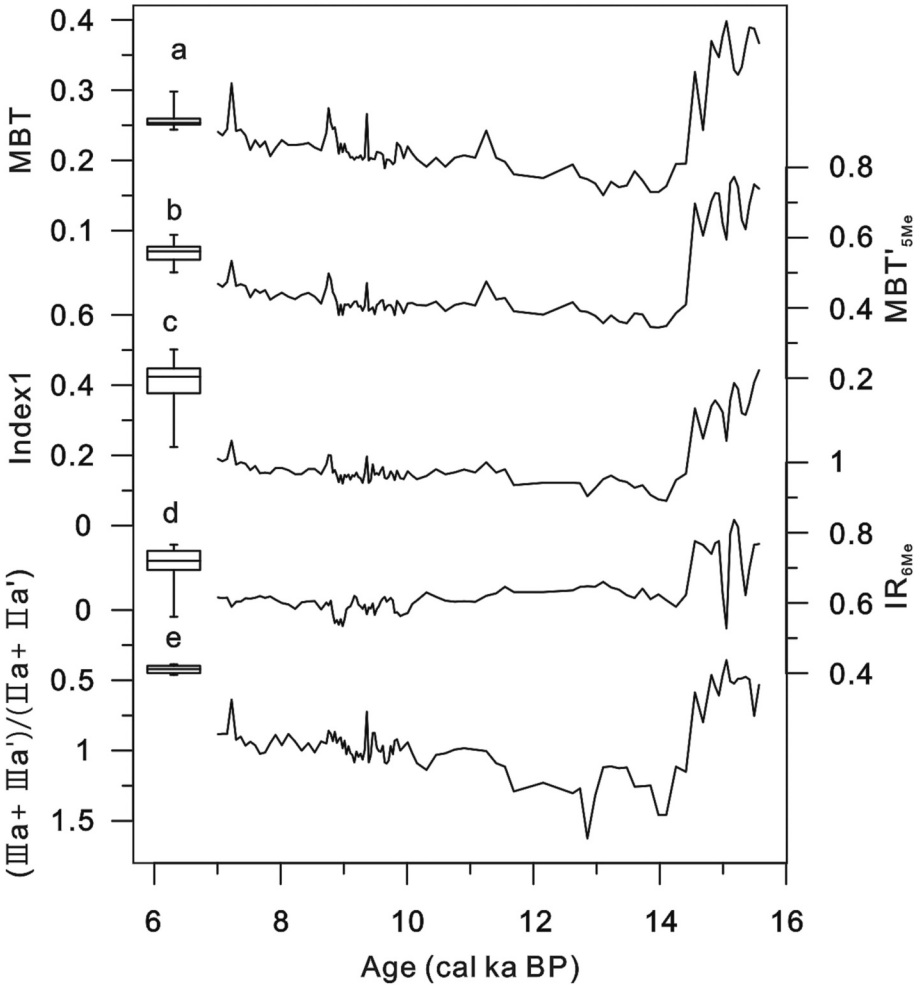

Fig. 3. Variations in MBT (a), MBT'$_{5Me}$ (b), Index1 (c), IR$_{6Me}$ (d), and (IIIa+ IIIa')/(IIa + IIa') ratio (e) from Lake Chenghai, The box–whisker plots indicate the values from surface lacustrine sediments.

latter changed significantly at ~14.6 cal ka BP. The tetramethylated brGDGTs accounted for 35.2% on average in down-core sediments from 15.6 to 14.6 cal ka BP but decreased to 20.9% from 14.4 to 7.0 cal ka BP. In contrast, the fractional abundance of hexamethylated brGDGTs accounted for 17.5% during the first period and increased to 31.6% during the second period.

Indices *MBT*, *MBT'*$_{5Me}$, *Index1*, *IR*$_{6Me}$, and ∑IIIa/∑IIa for the surface lacustrine sediments had ranges of 0.24–0.30, 0.50–0.61, 0.22–0.50, 0.56–0.77 and 0.39–0.46, respectively (Fig. 3). *MBT*, *MBT'*$_{5Me}$ and *Index1* values for the down-core sediments were significantly positively correlated. These values were higher during 15.6–14.6 cal ka BP, with means of 0.35, 0.70, and 0.35, respectively. In contrast, *MBT*, *MBT'*$_{5Me}$, and *Index1* values were lower during 14.4–7.0 cal ka BP, with values of 0.21 ± 0.03, 0.41 ± 0.03, and 0.14 ± 0.03, respectively. *IR*$_{6Me}$ ratios were relatively higher with a mean of 0.73 during 15.6–14.6 cal ka BP, while relatively stable in the range of 0.53–0.66 during 14.4–7.0 cal ka BP. The ∑IIIa/∑IIa ratio varied between 0.36 and 0.80 during 15.6–14.6 cal ka BP, whereas it ranged from 0.64 to 1.62 during 14.4–7.0 cal ka BP.

4. Discussion

4.1. Source and hydrological influences on brGDGT distributions

Previous studies have shown that the comparison of brGDGT distributions between lacustrine sediments and surrounding soils is an effective approach for identifying brGDGT sources within lacustrine environments (Dang et al., 2018; Martínez-Sosa et al., 2021; Russell et al., 2018; Sun et al., 2011). However, we did not collect the available surrounding soils from the catchment of Lake Chenghai, because of their low brGDGT concentrations. To help constrain brGDGT sources to the lacustrine sediments in Lake Chenghai, we compared the brGDGT distributions of Lake Chenghai sediments with previously published surface lacustrine sediments and mineral soils from China (Fig. 4). The ternary diagram shows that the brGDGT distributions of the Lake Chenghai sediments are comparable to those surface lacustrine sediments from China (Fig. 4). In contrast, the distribution of brGDGTs exhibited remarkable differences between lacustrine sediments and mineral soils from China, although the soil dataset covered a greater diversity in geography and climate (Fig. 4). In particular, lacustrine sediments had fewer tetramethylated and more pentamethylated brGDGTs than mineral soils, which is consistent with earlier reports (Sun et al., 2011; Yao et al., 2020; Zhao et al., 2021). The significant difference in the distribution suggests that brGDGTs in Lake Chenghai might be predominantly derived from an *in-situ* source, but the possible contribution of soil brGDGTs can not be entirely ignored.

The ∑IIIa/∑IIa ratio was originally developed to identify brGDGT sources in marine sediments, because most soils have a ratio lower than 0.59, while most marine sediments have a ratio higher than 0.92 (Xiao et al., 2016). Recently, this ratio has been applied to lacustrine environments (Cao et al., 2020; Martin et al., 2019; Zhang et al., 2022). In an alpine lake (Lake Cuoqia) from southwest China, the ∑IIIa/∑IIa ratio in sediments (1.36 ± 0.49) was much higher than that in catchment soils (0.22 ± 0.13), suggesting a substantial *in-situ* production of brGDGTs (Zhang et al., 2022). However, the Lake Chenghai sediments were characterized by a wide range of ∑IIIa/∑IIa ratios (0.36–1.62),

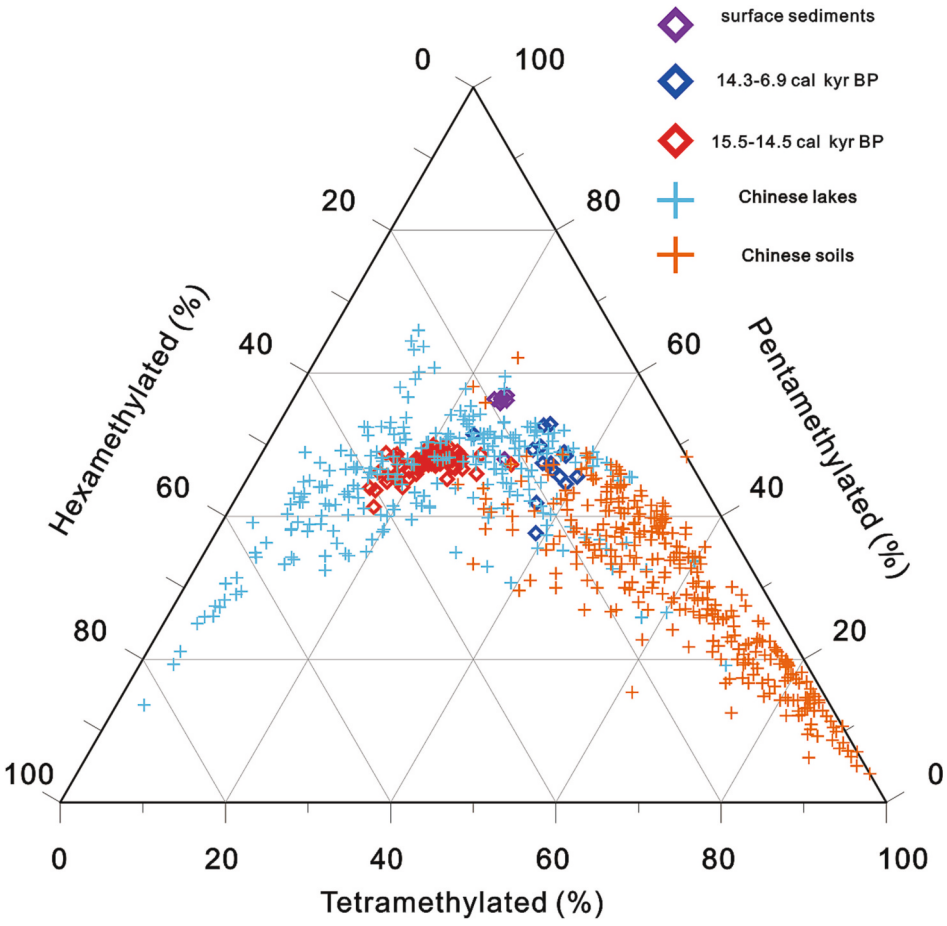

Fig. 4. Ternary diagram of the relative abundance of the tetramethylated, pentamethylated, and hexamethylated brGDGTs from surface and down-core sediments in Lake Chenghai, Chinese soils (De Jonge et al., 2014; Dearing Crampton-Flood et al., 2020; Ding, 2015; Lei et al., 2016; Wang et al., 2016; Xiao, 2015), and surface lacustrine sediments (Dang, 2018; Kou, 2022; Li, 2017; Wang, 2021; Yao, 2020; Zhao, 2021).

indicating a contribution of soil brGDGTs that could be variable through time. The lower ∑IIIa/∑IIa ratios occurred during 15.6–14.6 cal ka BP, corresponding well with the extreme low lake level recorded by the authigenic carbonate $\delta^{18}O$ (Sun et al., 2019). A possible reason for this is that less vegetation cover and exposure of the soil surface led to a significant contribution from the soil brGDGTs during the dry period. Similarly, changes in vegetation cover of climatic and/or anthropogenic origins in recent decades have increased soil erosion in the catchment and contributed to a significantly higher proportion of soil brGDGTs. However, we observed that low ∑IIIa/∑IIa ratios in the surface lacustrine sediments from East Asia, East Africa and other tropical regions (Dang et al., 2018; Russell et al., 2018; Zhao et al., 2023). Therefore, the ∑IIIa/∑IIa ratio seemed to be not a suitable proxy to distinguish the brGDGT sources in Lake Chenghai sediments.

Another possible explanation for the significant changes in the brGDGT distributions in the sediments of Lake Chenghai is the rapid lake expansion at ~14.6 cal ka BP (Sun et al., 2019). Previous studies have shown that water depth and dissolved oxygen are important variables that influence brGDGT-producing bacterial communities and productivity in lacustrine environments (Russell et al., 2018; Stefanescu et al., 2021; Weber et al., 2018; Wu et al., 2021; Yao et al., 2020). Russell et al. (2018) found significant correlations between the brGDGT distribution and water depth in East African lakes; however, the influence on the brGDGT distribution might be masked by the large temperature gradient and correlations among environmental variables. The fractional abundance of IIIa in suspended particulate matter was much higher in the deeper anoxic hypolimnion than in the shallower oxic epilimnion, as observed in volcanic lakes in northeast China and Lake Lugano in Europe (Weber et al., 2018; Yao et al., 2020). Stefanescu et al. (2021) found that shallow lakes in North America, with water depths below 3 m, exhibited higher fractional abundances of tetramethylated brGDGTs. Additionally, bacteria producing 5-methyl brGDGTs preferentially live in anoxic environments, whereas bacteria producing 6-methyl brGDGTs preferentially thriving in oxic conditions (Weber et al., 2018; Wu et al., 2021). The rapid decrease in IR_{6Me} ratios at approximately 14.6 cal ka BP was generally consistent with an increase in the lake level. Therefore, greater lake depth resulting from the strengthening of the summer monsoon would change the brGDGT-producing bacterial communities, which should be considered when discussing paleotemperature reconstructions.

4.2. Calibration selection and temperature reconstruction

BrGDGTs have been regarded as potential temperature indicators in various lacustrine environments, and numerous calibrations have been developed at both the regional and global scales (Dang et al., 2018; Martínez-Sosa et al., 2021; Russell et al., 2018; Stefanescu et al., 2021; Zhao et al., 2023; Zhao et al., 2021). Russell et al. (2018) initially established paleotemperature calibrations based on the separate quantification of 5- and 6-methyl brGDGTs in an East African lake dataset.

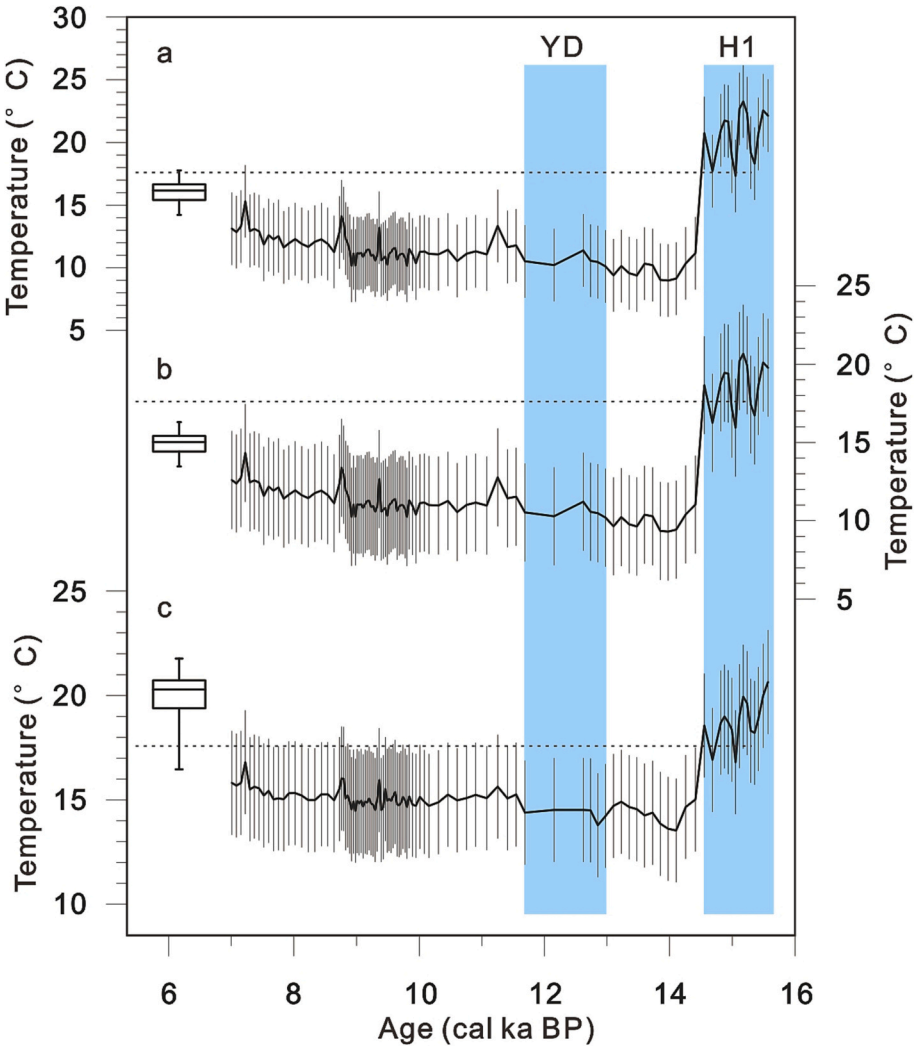

Fig. 5. Comparison of temperature reconstructed using different calibrations: using the lacustrine MBT'_{5ME} calibration by (a) Martínez-Sosa et al. (2021): MAAT = (MBT'_{5Me} - 0.075)/ 0.03, and (b) Zhao et al. (2023): MAAT = 26.49× MBT'_{5Me} + 0.2, respectively; (c) using the Index1 calibration by Zhao et al. (2021): MAAT = 19.11 the Index12.2. The box–whisker plots indicate the values from surface lacustrine sediments. Error bars represent the 1-sigma uncertainty based on the root square mean error of the calibrations, and dash lines represent the modern mean annual temperature. The Heinrich 1 (H1) and Younger Dryas (YD) are indicated by the horizontal shading.

Martínez-Sosa et al. (2021) and Zhao et al., (2023) found that the global MBT'$_{5Me}$-temperature calibrations for lacustrine sediments were generally consistent with that for East African lakes. Considering the similar climatic backgrounds of East Africa and southwest China, Zhao et al. (2021) combined nine lakes, including Lake Chenghai in southwest China, and proposed a revised calibration for tropical and subtropical lakes. In this study, we tested three temperature calibrations for Lake Chenghai sediments because of their better statistical results and more extensive sampling sites.

Using the global MBT'$_{5Me}$-based calibration of Martínez-Sosa et al. (2021), the reconstructed warm season temperatures varied between 14.2 and 17.8 °C, with a mean of 16.1 °C (Fig. 5). Because the monthly atmospheric temperature does not drop below 0 °C in the low altitudes in southwest China, the results matched well with the instrumental MAAT (17.6 °C). The new global calibration of Zhao et al., (2023) resulted in relatively low temperature estimates (15.0 ± 0.9 °C). This difference might be due to the incorporation of more tropical lakes with different water chemistries than in the previous study. Application of the Zhao et al. (2021) Index1-based calibration showed that MAAT varied between 16.5 and 21.8 °C, with a mean of 20.0 °C, slightly higher than the instrumental MAAT (Fig. 5). These results further support the dominant contribution of brGDGTs originating from *in-situ* production within the modern lake system of Lake Chenghai, and demonstrate the potential of previously published lacustrine calibrations to Lake Chenghai downcore sediments.

The three temperature calibrations at Lake Chenghai produced similar temperature changes during the deglaciation and early Holocene, which were characterized by a high temperature period during 15.6–14.6 cal ka BP (Fig. 5). The reconstructed temperature with global MBT'$_{5Me}$-temperature calibrations then decreased by an unrealistic 7–9 °C, while the Index1-based temperature decreased by approximately 3 °C. During 14.4–7.0 cal ka BP, the MBT'$_{5ME}$-based MAAT values were more variable than those based on Index1, although all series exhibited a consistent warming trend. As discussed above, the bacteria producing 5-methyl brGDGTs were more abundant under anaerobic conditions; thus, changes in the water level could significantly affect MBT'$_{5Me}$ and, in turn, overprint the temperature signal. In contrast, Index1-based reconstruction may produce more accurate temperature estimates for Lake Chenghai. Two cold reversals were detected in the Index1-based MAAT during the deglacial period, corresponding well to the Older Dryas (OD) cold event and the YD period of the Greenland ice core records within age uncertainty (Fig. 6, Rasmussen et al., 2014). This suggests that the temperature of Lake Chenghai is sensitive to global deglacial climate change. Furthermore, the onset of the Holocene was indicated by a rise in the Index1-based MAAT, and the reconstructed MAAT during the early Holocene (11.5–7.0 cal ka BP) was ~2.5 °C cooler than modern temperature.

4.3. Regional comparison and temperature seasonality

The reconstructed MAAT from Lake Chenghai indicated moderate cooling at the beginning of the YD event, punctuating the overall warming of the last deglaciation (Fig. 6). YD cooling has been identified in a growing number of lacustrine records from southwest China, with different magnitude of temperature change (Opitz et al., 2015; Tian et al., 2019; Xiao et al., 2014; Zhang et al., 2022; Zhang et al., 2019; Zhao et al., 2021). For example, a high-resolution pollen record from Lake Haligu suggested that the temperature was unstable during the YD period in the Hengduan Mountains, reconstructing a decrease of 4.8 °C in the MAAT (Yao et al., 2020). Pollen record from Lake Naleng suggested that MAAT decreased from −2.2 to −5 °C during the period 13.0–11.5 cal ka BP, to 2 °C colder than the temperature during the initial deglaciation (Opitz et al., 2015). However, chironomid fossils from Lake Tiancai showed a slight YD event from the perspective of summer temperatures (Fig. 6e, Zhang et al., 2019). Similarly, brGDGT-derived temperatures from Lake Cuoqia only recorded a transitory cooling of ~0.5 °C during 12.2–11.5 cal ka BP, due to the lacustrine brGDGT distributions being potentially biased towards the mean temperature of months above freezing at high altitudes (Zhang et al., 2022). Furthermore, existing sea-surface temperature records from the northern Indian Ocean indicated a brief cooling episode during the YD event (Govil and Divakar Naidu, 2011; Mohtadi et al., 2016; Rashid et al., 2007; Tierney et al., 2015). In contrast to the well-documented YD, the centennial OD cool event was less stressed in southwest China and adjacent regions. Several stalagmite $\delta^{18}O$ records from this region are characterized by higher $\delta^{18}O$ during the OD (Fig. 6f, Dykoski et al., 2005; Sinha et al., 2005). The similar pattern of variation between the brGDGT-based temperature and stalagmite $\delta^{18}O$ values suggests that both the temperature and precipitation in the Indian summer monsoon region are closely linked to the North Atlantic climate. Nevertheless, these lines of evidence suggest that temperature changes during the late deglaciation were coherent in the Northern Hemisphere.

The relatively lower early Holocene MAAT compared to present from Lake Chenghai can be supported by brGDGT records from adjacent lakes Tengchongqinghai, Lugu, Tiancai and Cuoqia (Fig. 6b–d, Feng et al., 2022; Zhang et al., 2022; Zhao et al., 2021). However, previous studies based on chironomids and pollen records have mainly assumed that the early Holocene climate was warmer in southwest China (Chen et al., 2020; Jiang et al., 2019; Shen et al., 2006; Zhang et al., 2017a). Holocene summer temperatures reconstructed using chironomid fossils from Lake Tiancai indicate that a temperature maximum occurred at 9–5 cal ka BP and a general cooling trend towards the present (Zhang et al., 2017a). Chen et al. (2020) recently stacked summer temperatures and MAAT reconstructions based on 29 pollen records on the Qinghai-Tibetan Plateau, which generally showed similar Holocene cooling patterns with only minor differences in timing and amplitude. Differences in the proxy-based temperature reconstruction largely depended on the length of the growing season. Specifically, chironomids have been used to reconstruct summer temperature changes at mid-high latitudes and/or high altitudes, as these environmental factors play a critical role in adult emergence during the chironomid life cycle (Heiri et al., 2011; Zhang et al., 2017b). A similar case can be applied to pollen records in southwest China, where the sensitivity of plant responses to summer temperatures depends on the integrated effects of maximum warmth, growing-season length, and precipitation changes influenced by the Indian summer monsoon (Chen et al., 2014; Marsicek et al., 2018). In contrast, pollen records from both Lake Wuxu and Lake Muge in the southeastern margin of the Qinghai-Tibetan Plateau showed that the cold-tolerant *Betula* reached a maximum in the vertical vegetation belt during the early Holocene, suggesting that the relatively cooler early Holocene might have been the result of colder winter in southwest China (Ni et al., 2019; Zhang et al., 2016).

The assessment of spatial variations in temperature across different altitudes is useful for evaluating the amplification of elevation and seasonal biases in proxy-based temperature reconstruction (Chu et al., 2017; Marsicek et al., 2018; Yan et al., 2021; Zhang et al., 2022). In this study, the relationship between seasonal temperature anomalies and elevation in southwest China during the late deglaciation-Holocene transition was primarily examined by comparing the brGDGT-based MAAT from Lake Chenghai (1496 m), Lake Tengchongqinghai (1885 m, Zhao et al., 2021), Lake Lugu (2685 m, Zhao et al., 2021) and Lake Tiancai (3898 m, Feng et al., 2022), and a high-resolution chironomid-based summer temperature from Lake Tiancai (Zhang et al., 2017a; Zhang et al., 2019). As expected, the MAAT changes during the transition in the high mountainous regions were larger than those in the low basins (Fig. 6). The warming rate of MAAT was 0.17 °C kyr^{-1} around Lake Chenghai, 0.10 °C kyr^{-1} around Lake Tengchongqinghai, 0.26 °C kyr^{-1} around Lake Lugu and 0.33 °C kyr^{-1} around Lake Tiancai (Fig. 6). Even considering the large geographic distances between these records, the more sensitive temperature change at higher elevations on a long-term scale is consistent with results from tropical high altitude mountains (Barrows et al., 2011; Loomis et al., 2017). Furthermore, much

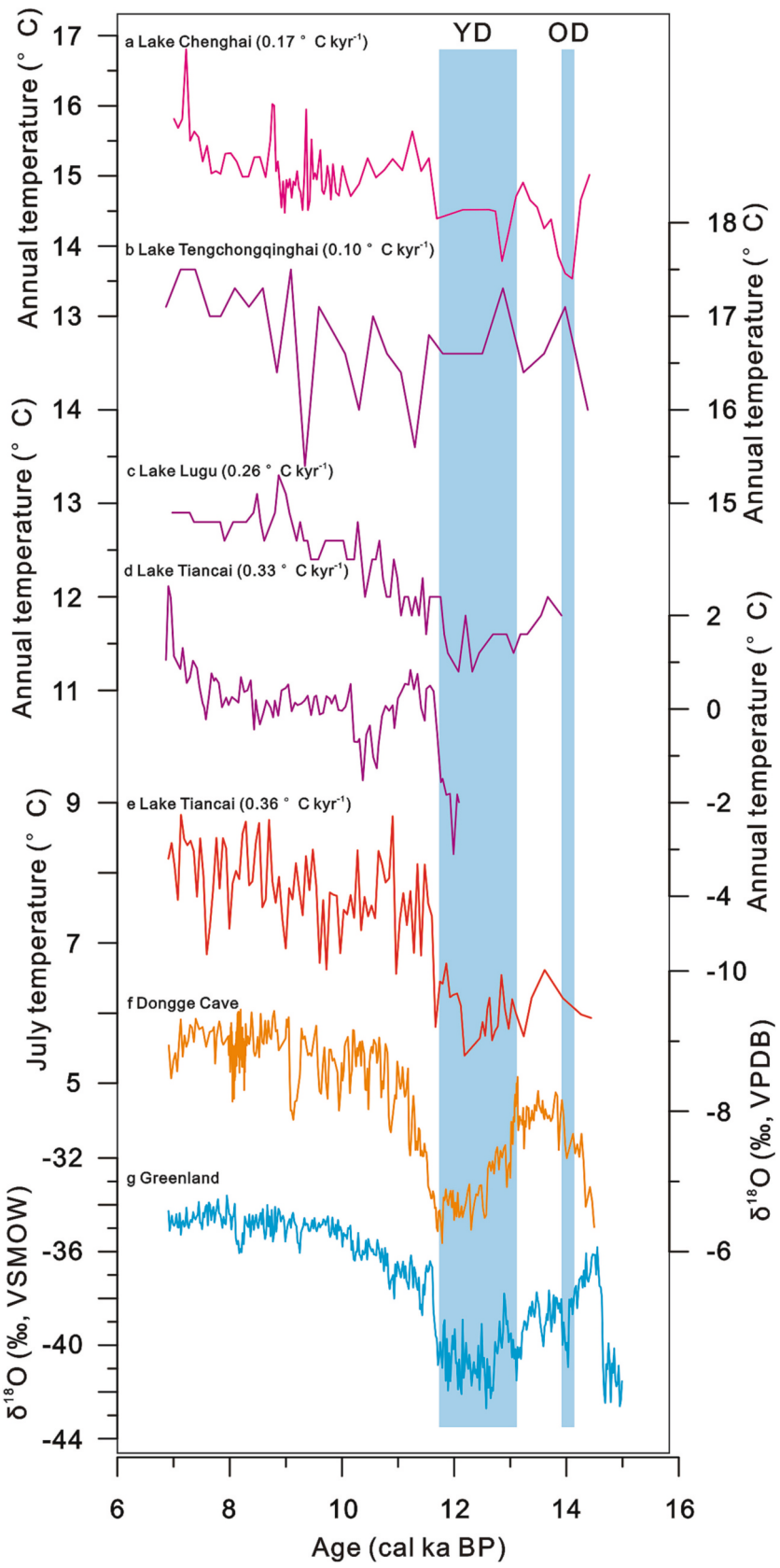

Fig. 6. BrGDGT-based MAAT reconstructions from southwest China of varying elevations: (a) Lake Chenghai; (b) Lake Tengchongqinghai (Zhao et al., 2021); (c) Lake Lugu (Zhao et al., 2021); (d) Lake Tiancai (Feng et al., 2022). The temperature records are compared to summer temperature based on chironomid fossils from Lake Tiancai (e, Zhang, 2017a, 2019); the stalagmite $\delta^{18}O$ record from Dongge Cave (f, Dykoski et al., 2005) and the $\delta^{18}O$ record from Greenland (g, Rasmussen et al., 2014). The older Dryas (OD) and Younger Dryas (YD) are indicated by the horizontal shading.

higher rates of warming in chironomid-based summer temperatures were found around Lake Tiancai (0.36 °C kyr^{-1}, Zhang et al., 2017a; Zhang et al., 2019). It must be noted that while the site-specific brGDGT-temperature calibration applied to Lake Tiancai represents MAAT, other calibrations are biased towards ice-free seasons (Feng et al., 2022). Therefore, the large differences can only be partially attributed to the proxy calibration methods.

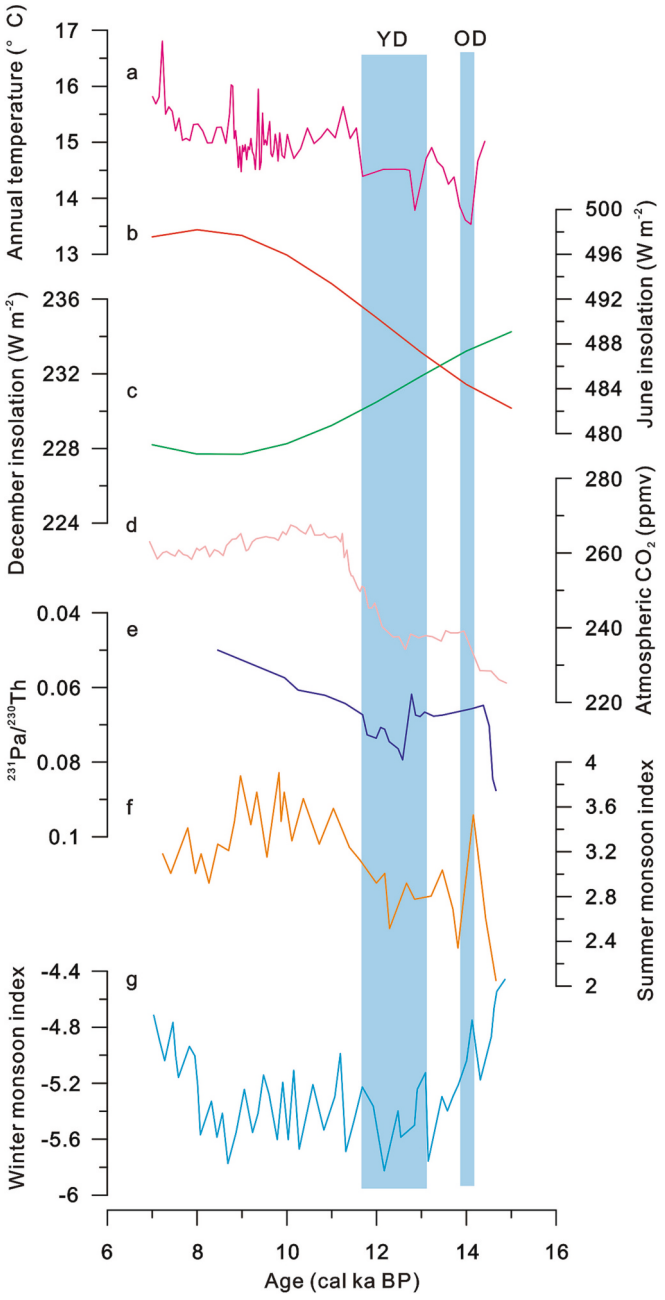

Fig. 7. Comparison of the brGDGT-based MAAT record from Lake Chenghai (a) with potential forcing factors. (b) Summer and (c) winter insolation curve for 30 °C (Laskar et al., 2004); (d) Atmospheric CO_2 concentration from the EPICA Dome C ice core, Antarctica (Monnin et al., 2004); (e) ^{231}Pa/^{230}Th record of North Atlantic, a proxy for AMOC (McManus et al., 2004); (f) and (g) Modelled summer and winter monsoon in East Asia response included forcings of CO_2, solar insolation, meltwater flux and ice sheets using the transient simulations (Wen et al., 2016). The older Dryas (OD) and Younger Dryas (YD) are indicated by the horizontal shading.

4.4. Potential forcing mechanisms of temperature variability and implication

The synchronous brGDGT-derived MAAT record from Lake Chenghai with temperature variability in mid- and high-latitudes in the Northern Hemisphere suggests that increased CO_2 concentrations and an inter-hemispheric redistribution of heat were the primary climate forcing during the last deglaciation-Holocene transition (Fig. 7d, Clark et al., 2012; Shakun et al., 2012). Superimposed on the long-term warming trend, the two cold spells, known as the OD and YD events, are probably linked to variations in meltwater discharge to the North Atlantic (Stanford et al., 2006). The resumption of the Atlantic meridional overturning circulation (AMOC) transported a massive amount of oceanic heat to high northern latitudes at the onset of the Bølling-Allerød warming period, leading to the most rapid deglacial reduction of continental ice sheets and sea-level rise, meltwater pulse 1a (MWP 1a) at ~14.1 cal ka BP (Bard et al., 1996; Lambeck et al., 2014; McManus et al., 2004). The suppression of AMOC was not recorded by the ^{231}Pa/^{230}Th record from the subtropical North Atlantic, potentially because of the migration of the deep-water formation north of the Greenland-Iceland-Scotland ridge (Fig. 7e, McManus et al., 2004). Conversely, iceberg discharge during the YD, although small enough to remain undetectable in the sea-level record, might have caused a pronounced collapse of deep-water formations (Fig. 7e, McManus et al., 2004). The slowdown in deep-water formation reduces meridional northward heat transport, resulting in the abrupt cooling of the North Atlantic and the surrounding Eurasian continent through the migration of the Intertropical Convergence Zone (ITCZ), Hadley circulation, and westerly jet stream (Chu et al., 2017; Clark et al., 2012; Sun et al., 2012; Zhang et al., 2017a).

The Asian monsoon is the most active and powerful circulation system in the Northern Hemisphere and plays an important role in regulating climate variability through the exchange of water vapor and energy between low and high latitudes (Clark et al., 2012). It is well recognized that the winter monsoon is mainly controlled by ice volume (Sun et al., 2012). The expansion of the sea ice extent over the North Atlantic during the YD event favors the expansion of the Siberian High pressure and intensifies the winter monsoon in the lower troposphere (Chu et al., 2017; Wen et al., 2016). Modern instrumental observations and historical records indicate that stronger winter monsoons in southern China are often accompanied by extremely cold winters and heavy snowfall (Zheng et al., 2012). Although long-term continuous high-resolution winter monsoon and snowfall records are limited to the study region, t supporting diatom evidence from Lake Yunlong suggests that heavy snowfall was prolonged during the YD on the southeastern Tibetan Plateau (Wang et al., 2018). As a result, we speculate that YD cooling was amplified in the high-altitude mountains of southwest China due to snow-albedo feedback during the cold seasons (Pepin et al., 2015; Yan et al., 2021). In addition, the southward migration of the inter-tropical convergence zone weakens the summer monsoon, leading to a reduction in monsoon flow in the Indian Ocean and summer cooling in southwest China (Zhang et al., 2019). Therefore, the OD and YD cooling in southwest China are mainly attributed to the combined opposite responses of the winter and summer monsoons to North Atlantic meltwater forcing.

It has been suggested that the early Holocene MAAT lower than present in southwest China is linked to strong seasonality dominated by very cold winters (Feng et al., 2022; Zhang et al., 2022). Changes in Holocene winter temperatures in the northern high latitudes were influenced by winter insolation, atmospheric greenhouse gases, and ice-sheet extent (Fig. 7c and d, Baker et al., 2017; Meyer et al., 2015). Lower winter insolation, lower atmospheric CO_2, and remnant high-latitude continental ice-sheets may have resulted in relatively cold winter temperatures and strengthened the Siberian High in the northern high latitudes during the early Holocene (Baker et al., 2017; Marsicek et al., 2018; Meyer et al., 2015). Likewise, model simulations suggested that the early Holocene winter monsoon was the strongest over the past 21 ka

and brought relatively cold air masses to China (Fig. 7g, Wen et al., 2016). For example, the MAAT based on soil isoprenoid tetraethers from Tianshan Mountains was ~10 °C colder than the present (Duan et al., 2022). However, the summer monsoon also reached its maximum during the early Holocene, resulting from a peak in summer insolation in the Northern Hemisphere (Fig. 7f, Wen et al., 2016; Zhang et al., 2017a). Sensitive warming in summer during the deglaciation-Holocene transition in southwest China was also likely controlled by atmospheric water vapor content (Zhang et al., 2019). The higher atmospheric humidity would result in a slight shoaling of the temperature lapse rate towards moist adiabat in the lower troposphere during the early Holocene. In tropical Africa, the decrease in temperature lapse rate from 6.7 °C km^{-1} during the last glacial maximum to 5.8 °C km^{-1} in the Holocene led to a 2–3 °C warming in the high altitudes (Loomis et al., 2017). This line of evidence suggests that a slight modification in the temperature lapse rate would accelerate summer warming around Lake Tiancai. Therefore, the divergent influence of the winter and summer monsoons reduced MAAT variations during the early Holocene.

Furthermore, our new MAAT record supports the ability of models such as the Community Climate System Model 3 to capture global annual mean warming during the Holocene but contradicts the general cooling trend in the global marine and terrestrial temperature stack (Kaufman et al., 2020; Liu et al., 2014; Marcott et al., 2013; Osman et al., 2021). This discrepancy can be partly attributed to the seasonality of the proxy records and the uneven geographical distribution of the Holocene temperature database (Marsicek et al., 2018; Osman et al., 2021). For example, global Holocene cooling in the temperature stacks of Marcott et al. (2013) was largely due to a few temperature records from the North Atlantic and was opposed by warming at low latitudes. Recently, Marsicek et al. (2018) reconstructed a long-term Holocene warming trend in North America and Europe that persisted until around the past two millennia based on pollen records. However, without the comprehensive consideration of brGDGT sources, limnological conditions, and species compositions, brGDGT-based reconstructions using different calibrations might either underestimate or overestimate the amplitude of temperature changes (Weber et al., 2018). In addition, feedback mechanisms such as clouds and atmospheric dust still require evaluation in current climate models (Bader et al., 2020). Therefore, new, detailed paleoclimate records and additional climate simulations are required to further understand the mechanisms and climate-forcing responses on various temporal and spatial scales.

5. Conclusions

In this study, brGDGT record from Lake Chenghai, southwest China, during the late deglaciation and early Holocene were investigated. The main source of brGDGTs was *in-situ* production and the distribution at ~14.6 cal ka BP corresponds to the rapid increase in lake level. An accurate and reliable MAAT record spanning the period 14.4–7.0 cal ka BP was obtained using a regional lacustrine calibration. The quantitative MAAT record displays a long-term warming trend during the late deglaciation-Holocene transition with a rate of 0.17 °C kyr^{-1}. Superimposed on this overall trend, cooling events corresponding to the OD and YD in the North Atlantic were registered in the Lake Chenghai record. The temperature reconstruction was in good agreement with previous brGDGT-based reconstructions, revealing a winter-biased and elevation-dependent MAAT change in southwest China. In addition to climate forcing such as solar insolation, greenhouse gases and meltwater discharge to the North Atlantic, we propose that winter and summer monsoons could have amplified temperature changes in high-altitude mountains through feedback from snow albedo and latent heat release. Our study supports the explanation for the Holocene temperature conundrum, which results from seasonal bias in proxy reconstructions and the scarcity of proxy records in large parts of low latitudes.

Declaration of Competing Interest

The authors declare that they have no known competing financial interests or personal relationships that could have appeared to influence the work reported in this paper.

Data availability

Data will be made available on request.

Acknowledgments

We express our gratitude to Dr. Steve Pratte for correcting this language. This research was financially supported by the National Natural Science Foundation of China (Grant Nos. 42025707 and 41888101), National Key Research and Development Program of China (Grant Nos. 2022YFF0801104 and 2016YFA0600502), and the Nanjing Institute of Geography and Limnology of the Chinese Academy of Sciences (Grant Nos. 2021NIGLAS-CJH03 and NIGLAS2022TJ01).

Appendix A. Supplementary data

Supplementary data to this article can be found online at https://doi.org/10.1016/j.gloplacha.2023.104238.

References

Bader, J., et al., 2020. Global temperature modes shed light on the Holocene temperature conundrum. Nat. Commun. 11 (1), 4726.
Baker, J.L., Lachniet, M.S., Chervyatsova, O., Asmerom, Y., Polyak, V.J., 2017. Holocene warming in western continental Eurasia driven by glacial retreat and greenhouse forcing. Nat. Geosci. 10 (6), 430–435.
Bard, E., et al., 1996. Deglacial sea-level record from Tahiti corals and the timing of global meltwater discharge. Nature 382 (6588), 241–244.
Barrows, T.T., Hope, G.S., Prentice, M.L., Fifield, L.K., Tims, S.G., 2011. Late Pleistocene glaciation of the Mt Giluwe volcano, Papua New Guinea. Quat. Sci. Rev. 30 (19), 2676–2689.
Cao, J., Rao, Z., Shi, F., Jia, G., 2020. Ice formation on lake surfaces in winter causes warm-season bias of lacustrine brGDGT temperature estimates. Biogeosciences 17 (9), 2521–2536.
Chen, F., et al., 2014. Holocene vegetation history, precipitation changes and Indian Summer Monsoon evolution documented from sediments of Xingyun Lake, southwest China. J. Quat. Sci. 29 (7), 661–674.
Chen, X., et al., 2019. Hydroclimatic influence on the salinity and water volume of a plateau lake in southwest China. Sci. Total Environ. 659, 746–755.
Chen, F., et al., 2020. Climate change, vegetation history, and landscape responses on the Tibetan Plateau during the Holocene: a comprehensive review. Quat. Sci. Rev. 243, 106444.
Chu, G., et al., 2017. The role of the Asian winter monsoon in the rapid propagation of abrupt climate changes during the last deglaciation. Quat. Sci. Rev. 177, 120–129.
Clark, P.U., et al., 2009. The last glacial maximum. Science 325 (5941), 710.
Clark, P.U., et al., 2012. Global climate evolution during the last deglaciation. Proc. Natl. Acad. Sci. U. S. A. 109 (19), E1134–E1142.
Dang, X., et al., 2018. Different temperature dependence of the bacterial brGDGT isomers in 35 Chinese lake sediments compared to that in soils. Org. Geochem. 119, 72–79.
Dang, X., Yang, H., Naafs, B.D.A., Pancost, R.D., Xie, S., 2016. Evidence of moisture control on the methylation of branched glycerol dialkyl glycerol tetraethers in semi-arid and arid soils. Geochim. Cosmochim. Acta 189, 24–36.
De Jonge, C., et al., 2014. Occurrence and abundance of 6-methyl branched glycerol dialkyl glycerol tetraethers in soils: Implications for palaeoclimate reconstruction. Geochim. Cosmochim. Acta 141, 97–112.
Dearing Crampton-Flood, E., Tierney, J.E., Peterse, F., Kirkels, F.M.S.A., Sinninghe Damsté, J.S., 2020. BayMBT: A Bayesian calibration model for branched glycerol dialkyl glycerol tetraethers in soils and peats. Geochim. Cosmochim. Acta 268, 142–159.
Ding, S., et al., 2015. Distribution of branched glycerol dialkyl glycerol tetraethers in surface soils of the Qinghai–Tibetan Plateau: implications of brGDGTs-based proxies in cold and dry regions. Biogeosciences 12 (11), 3141–3151.
Duan, Y., et al., 2022. General Holocene warming trend in arid Central Asia indicated by soil isoprenoid tetraethers. Global Planet. Change 215, 103879.
Dykoski, C.A., et al., 2005. A high-resolution, absolute-dated Holocene and deglacial Asian monsoon record from Dongge Cave, China. Earth Planet. Sci. Lett. 233 (1–2), 71–86.
Feng, X., et al., 2022. Evidence for a relatively warm mid-to late Holocene on the southeastern Tibetan Plateau. Geophys. Res. Lett. 49 (15) e2022GL098740.
Govil, P., Divakar Naidu, P., 2011. Variations of Indian monsoon precipitation during the last 32 kyr reflected in the surface hydrography of the Western Bay of Bengal. Quat. Sci. Rev. 30 (27–28), 3871–3879.

Heiri, O., Brooks, S.J., Birks, H.J.B., Lotter, A.F., 2011. A 274-lake calibration data-set and inference model for chironomid-based summer air temperature reconstruction in Europe. Quat. Sci. Rev. 30 (23), 3445–3456.
Jiang, W., et al., 2019. Synchronous strengthening of the Indian and East Asian Monsoons in response to global warming since the last deglaciation. Geophys. Res. Lett. 46 (7), 3944–3952.
Kaufman, D., et al., 2020. Holocene global mean surface temperature, a multi-method reconstruction approach. Scient. Data 7 (1), 201.
Kou, Q., et al., 2022. Distribution, potential sources, and response to water depth of archaeal tetraethers in Tibetan Plateau lake sediments. Chem. Geol. 601, 120825.
Lambeck, K., Rouby, H., Purcell, A., Sun, Y., Sambridge, M., 2014. Sea level and global ice volumes from the Last Glacial Maximum to the Holocene. Proc. Natl. Acad. Sci. 111 (43), 15296–15303.
Laskar, J., et al., 2004. A long-term numerical solution for the insolation quantities of the Earth. Astron. Astrophys. 428 (1), 261–285.
Lei, Y., Yang, H., Dang, X., Zhao, S., Xie, S., 2016. Absence of a significant bias towards summer temperature in branched tetraether-based paleothermometer at two soil sites with contrasting temperature seasonality. Org. Geochem. 94, 83–94.
Li, J.J., et al., 2017. Distribution of branched tetraether lipids in ponds from Inner Mongolia, NE China: Insight into the source of brGDGTs. Org. Geochem. 112, 127–136.
Liu, Z., et al., 2014. The Holocene temperature conundrum. Proc. Natl. Acad. Sci. 111 (34), E3501–E3505.
Loomis, S.E., et al., 2017. The tropical lapse rate steepened during the Last Glacial Maximum. Sci. Adv. 3 (1), e1600815.
Marcott, S.A., Shakun, J.D., Clark, P.U., Mix, A.C., 2013. A reconstruction of regional and global temperature for the past 11,300 years. Science 339 (6124), 1198–1201.
Marsicek, J., Shuman, B.N., Bartlein, P.J., Shafer, S.L., Brewer, S., 2018. Reconciling divergent trends and millennial variations in Holocene temperatures. Nature 554 (7690), 92–96.
Martin, C., et al., 2019. Impact of human activities and vegetation changes on the tetraether sources in Lake St Front (Massif Central, France). Org. Geochem. 135, 38–52.
Martínez-Sosa, P., et al., 2021. A global Bayesian temperature calibration for lacustrine brGDGTs. Geochim. Cosmochim. Acta 305, 87–105.
McManus, J.F., Francois, R., Gherardi, J.M., Keigwin, L.D., Brown-Leger, S., 2004. Collapse and rapid resumption of Atlantic meridional circulation linked to deglacial climate changes. Nature 428 (6985), 834–837.
Meyer, H., et al., 2015. Long-term winter warming trend in the Siberian Arctic during the mid- to late Holocene. Nat. Geosci. 8 (2), 122–125.
Mohtadi, M., Prange, M., Steinke, S., 2016. Palaeoclimatic insights into forcing and response of monsoon rainfall. Nature 533 (7602), 191–199.
Monnin, E., et al., 2004. Evidence for substantial accumulation rate variability in Antarctica during the Holocene, through synchronization of CO_2 in the Taylor Dome, Dome C and DML ice cores. Earth and Planet. Sci. Lett. 224 (1–2), 45–54.
Naafs, B.D.A., Gallego-Sala, A.V., Inglis, G.N., Pancost, R.D., 2017. Refining the global branched glycerol dialkyl glycerol tetraether (brGDGT) soil temperature calibration. Org. Geochem. 106, 48–56.
Ni, Z., et al., 2019. Contrasting effects of winter and summer climate on Holocene montane vegetation belts evolution in southeastern Qinghai-Tibetan Plateau, China. Palaeogeogr. Palaeoclimatol. Palaeoecol. 533, 109232.
Opitz, S., Zhang, C., Herzschuh, U., Mischke, S., 2015. Climate variability on the south-eastern Tibetan Plateau since the Lateglacial based on a multiproxy approach from Lake Naleng – comparing pollen and non-pollen signals. Quat. Sci. Rev. 115, 112–122.
Osman, M.B., et al., 2021. Globally resolved surface temperatures since the Last Glacial Maximum. Nature 599 (7884), 239–244.
Pepin, N., et al., 2015. Elevation-dependent warming in mountain regions of the world. Nat. Clim. Chang. 5 (5), 424–430.
Rashid, H., Flower, B.P., Poore, R.Z., Quinn, T.M., 2007. A ~25 ka Indian Ocean monsoon variability record from the Andaman Sea. Quat. Sci. Rev. 26 (19–21), 2586–2597.
Rasmussen, S.O., et al., 2014. A stratigraphic framework for abrupt climatic changes during the Last Glacial period based on three synchronized Greenland ice-core records: refining and extending the INTIMATE event stratigraphy. Quat. Sci. Rev. 106, 14–28.
Reimer, P.J., et al., 2013. IntCal13 and Marine13 radiocarbon age calibration curves 0–50,000 years cal BP. Radiocarbon 55 (4), 1869–1887.
Russell, J.M., Hopmans, E.C., Loomis, S.E., Liang, J., Sinninghe Damsté, J.S., 2018. Distributions of 5- and 6-methyl branched glycerol dialkyl glycerol tetraethers (brGDGTs) in East African lake sediment: Effects of temperature, pH, and new lacustrine paleotemperature calibrations. Org. Geochem. 117, 56–69.
Schouten, S., Hopmans, E.C., Sinninghe Damsté, J.S., 2013. The organic geochemistry of glycerol dialkyl glycerol tetraether lipids: a review. Org. Geochem. 54, 19–61.
Shakun, J.D., et al., 2012. Global warming preceded by increasing carbon dioxide concentrations during the last deglaciation. Nature 484, 49.
Shen, C., Liu, K.-b., Tang, L., Overpeck, J.T., 2006. Quantitative relationships between modern pollen rain and climate in the Tibetan Plateau. Rev. Palaeobot. Palynol. 140 (1–2), 61–77.
Sinha, A., et al., 2005. Variability of Southwest Indian summer monsoon precipitation during the Boiling-Allerod. Geology 33 (10), 813–816.
Sinninghe Damsté, J.S., et al., 2011. A 25,000-year record of climate-induced changes in lowland vegetation of eastern equatorial Africa revealed by the stable carbon-isotopic composition of fossil plant leaf waxes. Earth Planet. Sci. Lett. 302 (1–2), 236–246.
Stanford, J.D., et al., 2006. Timing of meltwater pulse 1a and climate responses to meltwater injections. Paleoceanography 21 (4).
Stefanescu, I.C., Shuman, B.N., Tierney, J.E., 2021. Temperature and water depth effects on brGDGT distributions in sub-alpine lakes of mid-latitude North America. Org. Geochem. 152, 104174.
Sun, Q., et al., 2011. Distributions and temperature dependence of branched glycerol dialkyl glycerol tetraethers in recent lacustrine sediments from China and Nepal. J. Geophys. Res. Biogeosci. 116.
Sun, Y., et al., 2012. Influence of Atlantic meridional overturning circulation on the East Asian winter monsoon. Nat. Geosci. 5 (1), 46–49.
Sun, W., et al., 2019. Abrupt changes in Indian summer monsoon strength during the last deglaciation and early Holocene based on stable isotope evidence from Lake Chenghai, southwest China. Quat. Sci. Rev. 218, 1–9.
Tian, L., et al., 2019. Synchronous change of temperature and moisture over the past 50 ka in subtropical southwest China as indicated by biomarker records in a crater lake. Quat. Sci. Rev. 212, 121–134.
Tierney, J.E., Pausata, F.S.R., deMenocal, P., 2015. Deglacial Indian monsoon failure and North Atlantic stadials linked by Indian Ocean surface cooling. Nat. Geosci. 9, 46.
Wang, L., et al., 2018. Prolonged heavy snowfall during the Younger Dryas. J. Geophys. Res. Atmos. 123 (24), 13748–13762.
Wang, H., et al., 2021. Salinity-controlled isomerization of lacustrine brGDGTs impacts the associated MBT_{5ME}' terrestrial temperature index. Geochim. Cosmochim. Acta 305, 33–48.
Wang, H., Liu, W., Lu, H., 2016. Appraisal of branched glycerol dialkyl glycerol tetraether-based indices for North China. Org. Geochem. 98, 118–130.
Weber, Y., et al., 2018. Redox-dependent niche differentiation provides evidence for multiple bacterial sources of glycerol tetraether lipids in lakes. Proc. Natl. Acad. Sci. 115 (43), 10926–10931.
Weijers, J.W.H., Schefuss, E., Schouten, S., Damste, J.S.S., 2007. Coupled thermal and hydrological evolution of tropical Africa over the last deglaciation. Science 315 (5819), 1701–1704.
Wen, X., Liu, Z., Wang, S., Cheng, J., Zhu, J., 2016. Correlation and anti-correlation of the East Asian summer and winter monsoons during the last 21,000 years. Nat. Commun. 7 (1), 11999.
Wu, J., Gagan, M.K., Jiang, X., Xia, W., Wang, S., 2004. Sedimentary geochemical evidence for recent eutrophication of Lake Chenghai, Yunnan, China. J. Paleolimnol. 32 (1), 85–94.
Wu, J., et al., 2021. Variations in dissolved O_2 in a Chinese lake drive changes in microbial communities and impact sedimentary GDGT distributions. Chem. Geol. 579, 120348.
Xiao, X., et al., 2014. Latest Pleistocene and Holocene vegetation and climate history inferred from an alpine lacustrine record, northwestern Yunnan Province, southwestern China. Quat. Sci. Rev. 86, 35–48.
Xiao, W., et al., 2015. Global calibration of a novel, branched GDGT-based soil pH proxy. Org. Geochem. 89-90, 56–60.
Xiao, W., et al., 2016. Ubiquitous production of branched glycerol dialkyl glycerol tetraethers (brGDGTs) in global marine environments: a new source indicator for brGDGTs. Biogeosciences 13 (20), 5883–5894.
Xiao, X., et al., 2018. Evidence of Holocene climatic change and human impact in northwestern Yunnan Province: High-resolution pollen and charcoal records from Chenghai Lake, southwestern China. Holocene 28 (1), 127–139.
Yan, T., et al., 2021. Elevational differences in Holocene thermal maximum revealed by quantitative temperature reconstructions at ~30° N on eastern Tibetan Plateau. Palaeogeogr. Palaeoclimatol. Palaeoecol. 570, 110364.
Yang, H., et al., 2015. The 6-methyl branched tetraethers significantly affect the performance of the methylation index (MBT ') in soils from an altitudinal transect at Mount Shennongjia. Org. Geochem. 82, 42–53.
Yao, Y.-F., et al., 2020. Evidence for climate instability during the Younger Dryas interval in the Hengduan Mountains, Yunnan, southwestern China. Palaeogeogr. Palaeoclimatol. Palaeoecol. 554, 109798.
Zhang, E., Wang, Y., Sun, W., Shen, J., 2016. Holocene Asian monsoon evolution revealed by a pollen record from an alpine lake on the southeastern margin of the Qinghai–Tibetan Plateau, China. Clim. Past 12 (2), 415–427.
Yao, Y., et al., 2020. Correlation between the ratio of 5-methyl hexamethylated to pentamethylated branched GDGTs (HP5) and water depth reflects redox variations in stratified lakes. Org. Geochem. 147, 104076.
Zhang, E., et al., 2017a. Holocene high-resolution quantitative summer temperature reconstruction based on subfossil chironomids from the southeast margin of the Qinghai-Tibetan Plateau. Quat. Sci. Rev. 165, 1–12.
Zhang, E.L., et al., 2017b. A chironomid-based mean July temperature inference model from the south-east margin of the Tibetan Plateau, China. Clim. Past 13 (3), 185–199.
Zhang, E., et al., 2019. Summer temperature fluctuations in southwestern China during the end of the LGM and the last deglaciation. Earth Planet. Sci. Lett. 509, 78–87.
Zhang, C., et al., 2022. Seasonal imprint of Holocene temperature reconstruction on the Tibetan Plateau. Earth Sci. Rev. 226, 103927.
Zhao, C., et al., 2021. Possible obliquity-forced warmth in southern Asia during the last glacial stage. Sci. Bull. 66 (11), 1136–1145.
Zhao, B., et al., 2023. Evaluating global temperature calibrations for lacustrine branched GDGTs: Seasonal variability, paleoclimate implications, and future directions. Quat. Sci. Rev. 310, 108124.
Zheng, J., Ding, L., Hao, Z., Ge, Q., 2012. Extreme cold winter events in southern China during AD 1650–2000. Boreas 41 (1), 1–12.